

## Determination of free carrier density and space charge layer variation in nanocrystalline In<sup>3+</sup> doped tin oxides using Fourier transform infrared spectroscopy

Christina Drake, Sameer Deshpande, and Sudipta Seal<sup>a)</sup>

Advanced Materials Processing and Analysis Center (AMPAC), University of Central Florida, 4000 Central Florida Boulevard, Orlando, Florida 32816, Mechanical Materials and Aerospace Engineering, University of Central Florida, 4000 Central Florida Boulevard, Orlando, Florida 32816, Department of Physics, University of Central Florida, 4000 Central Florida Boulevard, Orlando, Florida 32816

(Received 7 June 2006; accepted 26 August 2006; published online 6 October 2006)

A correlation between the surface reactions and the electrical response of doped nano-metal-oxide-semiconductors exposed to reducing gas is established using Fourier transform infrared (FTIR) spectroscopy. The effect of processing temperature on the microstructure evolution and the electronic conduction of the nanocrystalline In–SnO<sub>2</sub> is presented. Variation in the charge carrier density is correlated to the solid/gas reaction of In–SnO<sub>2</sub> in the nanodomain using the Drude-Zener theory including Spitzer and Fan's [Phys. Rev. **99**, 1893 (1955)] correction to accommodate for the quantum effects. Higher gas sensitivity for nanocrystalline size less than twice the space charge layer thickness is observed using *in situ* FTIR. © 2006 American Institute of Physics. [DOI: 10.1063/1.2360185]

Nanocrystalline metal oxides are widely used in energy conversion and storage, microelectronics, UV absorbance, and gas sensors.<sup>1</sup> However, the atomic scale interaction on the surface of metal oxide nanoparticles (NPs) with interacting gases is still unexplored. Fourier transform infrared (FTIR) spectroscopy can be used for studying such surface reactions and chemistry of the materials.<sup>2</sup> A few studies have shown that the variation in the infrared absorption of materials can be correlated to the variation in the free carrier densities.<sup>3</sup> The absorption by the free carriers on the surface in the space charge layer (SCL) may differ from that in the bulk.<sup>4</sup> Beer's law shows that the absorbance can be directly related to the absorption coefficient using<sup>5</sup>

$$I = I_0 \exp(-Kx), \quad (1)$$

where  $x$  is the thickness of the measured sample,  $I$  and  $I_0$  are the initial and transmitted intensities, respectively, and  $K$  represents the absorption coefficient. The Drude-Zener theory was used to calculate the conductivity as well as the major free carrier concentration using the relation<sup>5,6</sup>

$$K = \frac{1}{\epsilon_0 c_0 n} \cdot \frac{\sigma^2 q^2}{\omega^2 m^2 \mu^2} = \lambda_0^2 \cdot \frac{\sqrt{\mu_0}}{\sqrt{\epsilon_0}} \cdot \frac{Nq^3}{4\pi^2 n m^2 c_0^2 \mu}, \quad (2)$$

where  $N$  is the free carrier concentration (m<sup>-3</sup>),  $\sigma$  is the electrical conductivity (S/m),  $\omega$  is the angular frequency,  $m$  is the carrier effective mass (kg),  $\mu$  is the carrier mobility [m<sup>2</sup>/(V s)],  $n$  is the index of refraction, and  $\lambda_0$  is the wavelength in free space ( $1/n = \lambda/\lambda_0$ ). Equation (2) is valid when  $\omega\tau \gg 1$  and  $\sigma_0 \ll \omega\epsilon'$ , which holds up in the infrared region for most semiconductors. Equation (2) also considers that the infrared absorption of free carriers exhibits the Drude shape.<sup>7</sup> However, the Drude-Zener theory assumes classical statistics, which means that they assume that the energy absorbed by the carriers from the radiation is a small perturbation

compared with the mean carrier energy and this assumption can be written as  $h\omega \ll 2\pi kT$ .<sup>5</sup> However, quantum effects are important below a critical wavelength at a given temperature. Spitzer and Fan<sup>8</sup> have shown that the right-hand side of Eq. (2) for the absorption coefficient is needed to be corrected by

$$\sqrt{\frac{h\omega}{2\pi kT}} \quad \text{when } h\omega \geq 2\pi kT. \quad (3)$$

For low temperatures in the infrared region this relationship is required for nanomaterials. This leads to a  $\lambda^{3/2}$  variation with the wavelength for the conductivity of oxides in the infrared region.

Space charge layer of the nanocrystalline tin oxides for gas sensors can be tuned with doping various metallic elements. However, a systematic study of the major free carrier, as well as their concentration, in the SCL upon different doping amounts will give insight to the change in the conduction behavior. An increase in the surface oxygen vacant sites may further help surface dissociation reactions of gases to have immediate access to a site for electron injection. Doping with trivalent cations (such as Al<sup>3+</sup> and In<sup>3+</sup>) increases the number of intermediate energy levels created in the forbidden region of SnO<sub>2</sub>. This increases the conduction ability of the semiconductor by reducing the activation energy for conduction. Previous studies from the *author's group*<sup>9</sup> have shown an increase in the hydrogen sensitivity of In<sup>3+</sup> doped SnO<sub>2</sub>. This creates even more of the desired oxygen vacancies by substitution on a tin lattice site, which in equilibrium expects a 4+ charge to occupy the lattice site. This happens because a 3+ on a 4+ site makes the tin site feel a negative charge. To compensate, an oxygen vacancy will form which causes the previous oxygen site to experience a positive charge. This charge compensation enhances the gas sensing of doped SnO<sub>2</sub>. Charge modification occurred can be shown using *Kroger-Vink* notations as

<sup>a)</sup>Electronic mail: sseal@mail.ucf.edu

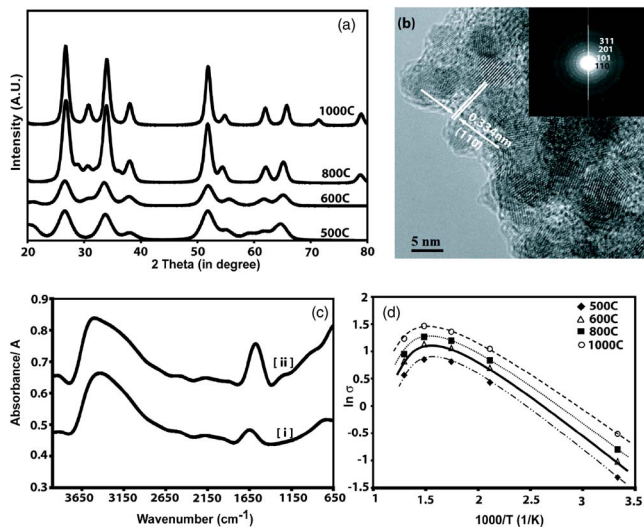
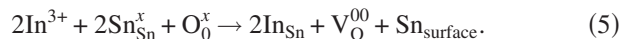
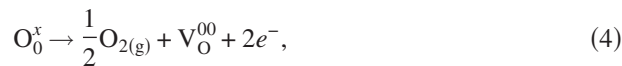


FIG. 1. (Color online) (a) X-ray diffraction of In doped  $\text{SnO}_2$  nanoparticles (NP) and (b) HRTEM of In doped  $\text{SnO}_2$  NPs; inset showing selected area electron diffraction confirming the growth of the In– $\text{SnO}_2$  particles in (110) plane of the cassiterite structure. (c) FTIR spectra of In doped  $\text{SnO}_2$  NP (i) before and (ii) after hydrogen exposure. (d) Effect of testing temperature on the conductivity variation of the NPs.



In this letter, we present the utilization of an *in situ* FTIR spectroscopy to study the effect of particle size of the doped and undoped nano-tin-oxide, its corresponding changes in the free carrier concentration, and subsequent variations in the SCL of the nanocrystalline  $\text{SnO}_2$ .

The phase transformation and the particle size variation of the doped  $\text{SnO}_2$  particles as a function of different calcination temperatures were studied using x-ray diffraction (Rigaku Model) with a  $\text{Cu K}\alpha 1$  radiation at 30 mA and 35 kV [Fig. 1(a)]. The sample calcined at 500 °C presents the dominant peaks at (110), (101), and (211), which further confirms the cassiterite structure of the nano- $\text{SnO}_2$ . The rutile crystal structure of  $\text{SnO}_2$  has a tetragonal unit cell with space-group symmetry of  $P42/mnm$ . The lattice constants are  $a=b=4.731 \text{ \AA}$  and  $c=3.189 \text{ \AA}$ . In  $\text{SnO}_2$ , Sn atoms are sixfold coordinated to threefold coordinated oxygen atoms. The (110) plane is the most stable plane of the low index faces<sup>10</sup> and cassiterite is the most stable phase of  $\text{SnO}_2$ . The (110) plane is the preferred growth plane, which performs the best in the gas sensing applications.<sup>11</sup> The surface morphology of the nanoparticles was determined by high resolution transmission electron microscopy (HRTEM) [Fig. 1(b)]. Particle sizes of samples calcined at 500, 600, 800, and 1000 °C observed using TEM were 5, 9, 20, and 40 nm, respectively, while the crystallite sizes calculated using conventional x-ray diffraction method for same samples were 4, 8, 15, and 30 nm, respectively. It can be observed that each individual grain is a single crystal, helping to reduce the barriers for conduction of the free carriers. Due to this very reason, the space charge variations can be considered the dominating conduction mechanism.

Figure 1(c) shows the variation of FTIR absorbance from doped  $\text{SnO}_2$ . An upward shift is observed in the absorbance spectra after exposure to  $\text{H}_2$ . Nano- $\text{SnO}_{2-x}$ , when ex-

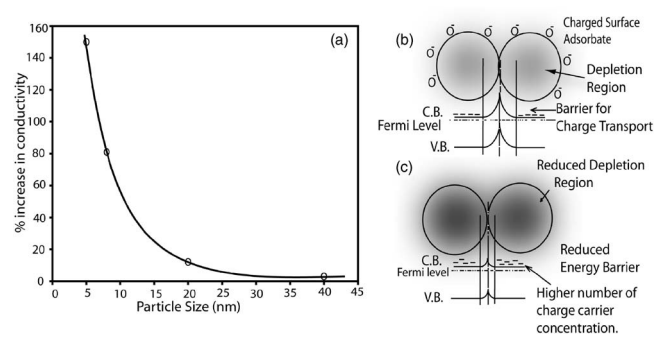


FIG. 2. (a) Impact of nanocrystalline size on the sensitivity of the In doped  $\text{SnO}_2$  on hydrogen exposure. (b) Formation of space charge layer (SCL) and corresponding band bending and energy barrier. (c) Reduction of space charge layer in SCL after injection of electron by hydrogen interaction of particles.

posed to air, oxygen molecules are physisorbed on the surface and take free electrons from  $\text{SnO}_{2-x}$  and a change occurs to  $\text{O}_{2\text{ ads}}^-$  or  $\text{O}_{\text{ ads}}^-$  species. When a reducing gas (e.g.,  $\text{H}_2$ ) comes in contact with nanoparticles, it is oxidized via reaction with the  $\text{O}_{2\text{ ads}}^-$  or  $\text{O}_{\text{ ads}}^-$  species, and, subsequently, electrons are reintroduced into the electron depletion layer. The electrons added to the space charge region of an *n*-type surface will lead to an increase in the absorption [see Fig. 1(c)].<sup>12</sup> The broad peak around  $3450 \text{ cm}^{-1}$  is due to physisorbed water (O–H bond stretching) or surface hydration.<sup>13</sup>

In Fig. 1(d), the conductivity increased with increasing temperature until a testing temperature of 500 °C, where a decrease was observed for all the samples. This is due to the switching of the conduction mechanism around this temperature from extrinsic to intrinsic conduction and a scattering effect from the two mechanisms is observed.<sup>14</sup> The slope of the straight part of the curve was taken as the activation energy for such conduction. From the promotion energy, the major charge carrier density is determined for In– $\text{SnO}_2$  samples calcined at 600, 800, and 1000 °C. The promotion energies are attributed to the electron transition from the monoionized oxygen vacancies to the conduction band which occur between 0.1 and 0.18 eV.<sup>15</sup> The calculated energies are 0.159 eV for 600 °C, 0.134 eV for 800 °C, and 0.11 eV for 1000 °C calcined nanocrystalline In– $\text{SnO}_2$ . There is a monotonous decrease in the energies as the temperature is increased from 600 to 1000 °C. This is likely due to the location of the bottom of the band gap relative to the shallow donor levels created by the oxygen vacancies. This band bending has been reported by other authors, caused by shifts in the Fermi level at different calcination temperatures.<sup>16</sup> It has been suggested that the Fermi level position may be affected by the presence of uncoordinated surface atoms.<sup>17</sup> For samples calcined at 500 °C, the promotion energy was found to be 0.31 eV.

The samples calcined at 500 and 600 °C showed the largest response to  $\text{H}_2$  [see Fig. 2(a)], though both mechanisms for conduction appear to be different at present. This result confirms that with decreasing crystallite size, there is an increased sensitivity to  $\text{H}_2$  in spite of the bulk conduction mechanism. This increase in response can be explained by the SCL model, Figs. 2(b) and 2(c). When oxygen molecules are physisorbed onto the surface of nano- $\text{SnO}_{2-x}$ , they receive electrons from  $\text{SnO}_{2-x}$  and a change occurs to  $\text{O}_{2\text{ ads}}^-$  or  $\text{O}_{\text{ ads}}^-$  species. Consequently, positive and negative space

TABLE I. Effect of operating temperature on free carrier densities observed from In doped SnO<sub>2</sub> NPs calcined at different temperatures.

Measured temperature (K)	Calcination T °C	Sample name (ITO)			
		500 °C	600 °C	800 °C	1000 °C
473.15		1.64	4.37	3.50	6.64
573.15	Vacancy concentration 10 <sup>23</sup> (1/m <sup>3</sup> )	6.64	8.00	7.44	6.36
673.15		5.01	7.21	7.50	10.8
773.15		9.94	9.94	2.59	5.03

charge layers form above and below the surface of SnO<sub>2-x</sub>. For nano-SnO<sub>2</sub> particles, a space charge layer of 3 nm has been reported.<sup>18</sup> As the grain size  $D$  approaches twice the depth of the SCL  $L$ , sensitivity to H<sub>2</sub> is drastically improved.<sup>19</sup> Twice this space charge layer thickness would correspond to approximately 6 nm for the desired grain size, not far from the 5 and 9 nm calculated for samples calcined at 500 and 600 °C, respectively. It has been previously calculated that addition of Al (3+) in SnO<sub>2</sub> increases the space charge layer from 3 to 90 nm. A similar effect is likely occurring in our In-SnO<sub>2</sub> system. In this case, both  $D$  and  $L$  were modified by controlling the grain size and introducing impurities to modify the surface, as well as the bulk electronic structure, of SnO<sub>2</sub>.<sup>18</sup>

Table I shows the effect of operating temperature on the free carrier density (using relationships 1–3) of the SnO<sub>2</sub> nanoparticles calcined at different temperatures. From Table I it can be inferred that overall variations of charge carrier density is in the range of 10<sup>23</sup>/m<sup>3</sup>–10<sup>24</sup>/m<sup>3</sup>, indicating extrinsic conduction at the lower testing temperatures. This is *very significant* to low temperature gas sensing. One of the possible ways to achieve low temperature sensing is to have higher oxygen vacancy concentrations. If the actual magnitude of the free carrier density does not reduce drastically with reducing temperature, then a nonequilibrium concentration of these vacancies has been achieved. This means that a high vacancy density can be maintained at lower temperatures.

The calculated free carrier density is lower than what has been reported for nano-SnO<sub>2</sub>,<sup>20,21</sup> in the range of 10<sup>26</sup>–10<sup>27</sup>/m<sup>3</sup>. Lower carrier density may be due to a grain boundary effect similar to that reported for doped ceria.<sup>22</sup> A likely place for the undoped indium to be located is at the grain boundaries or dispersed around the SnO<sub>2</sub> particles. If this is the scenario, conduction would be more inhibited at the grain boundaries only. Also, doping may have caused some of the dopants to pair with an oppositely charged oxygen vacancy, hindering the charge movement further. Another possibility is that our carrier density numbers reflect a characteristic of the space charge or the depleted region. The charge carriers held to a region near the surface by the potential well of a space charge region may have their mobility reduced by surface scattering.<sup>23</sup> This would change the value of the mean free path of the carriers which would explain the

discrepancy between the reported values and our calculated data. Further doping and structural studies are being carried out and will be reported in the future.

Trivalent In substitution into the nano-SnO<sub>2</sub> lattice structure has proven to be an excellent gas sensor at low temperatures. FTIR has shown the ability to calculate both the gas sensitivity and the electronic properties of nano-In-SnO<sub>2</sub> as a function of temperature. The controlling factors for enhanced gas sensing abilities at lower temperatures are extrinsic free carrier densities and NP size in relation to its Debye length.

The authors would like to thank NASA-Glenn, ASRC Corporation, and NSF-CTS for funding nanotechnology and sensor research and NSF—GK-12 fellowship.

- <sup>1</sup>S. Shukla, S. Seal, L. Ludwig, and C. Parish, *Sens. Actuators B* **97**, 256 (2004).
- <sup>2</sup>M.-I. Baraton and L. Merhari, *J. Eur. Ceram. Soc.* **24**, 1399 (2004).
- <sup>3</sup>N. Harrick, *Phys. Rev.* **103**, 1173 (1956).
- <sup>4</sup>N. Harrick, *J. Phys. Chem. Solids* **14**, 60 (1960).
- <sup>5</sup>A. F. Gibson, *J. Sci. Instrum.* **35**, 273 (1958).
- <sup>6</sup>M.-I. Baraton and L. Merhari, *Synthesis Reactivity Inorganic Metal-Organic and Nano-Metal Chemistry* **35**, 733 (2005).
- <sup>7</sup>N. J. Harrick, *Phys. Rev.* **125**, 1165 (1962).
- <sup>8</sup>W. G. Spitzer and H. Y. Fan, *Phys. Rev.* **99**, 1893 (1955).
- <sup>9</sup>S. Shukla, S. Patil, S. C. Kuiry, Z. Rahman, T. Du, L. Ludwig, C. Parish, and S. Seal, *Sens. Actuators B* **96**, 343 (2003).
- <sup>10</sup>J. Ahn, S. Kim, J. Park, and M. Huh, *Sens. Actuators B* **94**, 125 (2003).
- <sup>11</sup>P. Patil, R. Kwar, S. Sadale, and P. S. Chigare, *Thin Solid Films* **437**, 34 (2003).
- <sup>12</sup>G. Martinelli and M. Carotta, *Sens. Actuators B* **23**, 157 (1995).
- <sup>13</sup>F. Sensato, R. Custodio, M. Calatayud, A. Beltran, J. Andres, J. Sambrano, and E. Longo, *Surf. Sci.* **511**, 408 (2002).
- <sup>14</sup>A. R. West, *Basic Solid State Chemistry*, 2nd ed. (Wiley, Chichester, UK, 1999), Chap. 7, p. 27.
- <sup>15</sup>G. Ghiotti, A. Chiorino, and F. Prinetto, *Sens. Actuators B* **24-25**, 564 (1995).
- <sup>16</sup>T. Maffei, G. Owen, M. Penny, T. Starke, S. Clark, H. Ferkel, and S. Wilks, *Surf. Sci.* **520**, 29 (2002).
- <sup>17</sup>N. Yamazoe, *Sens. Actuators B* **5**, 7 (1991).
- <sup>18</sup>S. Kucheyev, T. Baumann, P. Sterne, Y. Wang, T. van Buuren, A. Hamza, L. Terminello, and T. Willey, *Phys. Rev. B* **72**, 035404 (2005).
- <sup>19</sup>H. Ogawa, M. Nishikawa, and A. Abe, *J. Appl. Phys.* **53**, 4448 (1982).
- <sup>20</sup>E. Rakhshani, Y. Makdisi, and H. A. Ramazaniyan, *J. Appl. Phys.* **83**, 1049 (1998).
- <sup>21</sup>H. I. Elim, W. Ji, and F. Zhu, *Appl. Phys. B: Lasers Opt.* **82**, 439 (2006).
- <sup>22</sup>R. Gerhardt and A. Nowick, *J. Am. Ceram. Soc.* **69**, 641 (1986).
- <sup>23</sup>J. R. Schrieffer, *Phys. Rev.* **97**, 641 (1955).